Chapter 3
Elastic Model of a Deformable Fingertip

3.1 Introduction

To date, much research has been done on the manipulation of objects by soft-fingered robotic hands. Most of these studies, particularly the earlier ones, focused only on contact mechanisms on various soft fingers. More recently, there has been an increase in the number of studies investigating the sensing mechanisms of the human hand and designing control systems in robotic applications to emulate the human capabilities that are applicable to robotic hands. Conventional studies, however, have not explicitly provided any analytical exploration of the simplicity in grasping and manipulating motions in terms of soft-fingered handling. It has therefore been very difficult to derive a fine elastic model of soft materials used in fingertips.

Yokokohji *et al.* proposed a control scheme with visual sensors that can cancel the frictional twist/spin moment at the contact point of soft fingertips and achieved stable grasping by spherical soft fingertips [YSY99, YSY00]. Maekawa *et al.* developed a finger-shaped tactile sensor covered with a soft, thin material and proposed a control algorithm based on tactile feedback using a sensor that requires no information about the geometry of the grasped object [MKT92, MTK$^+$92]. They managed to control the position of an object along a desired trajectory. In these papers, point-contacts were used to represent the constraints of rolling contact in their theoretical models, although the fingertips were made from a soft material such as rubber. Arimoto *et al.* verified the passivity of equations of motion for a total handling system using a Lagrangian function incorporating the elastic potential energy due to the deformation of soft fingertips [ANH$^+$00] and compensated for the gravity effect in 3D space [ADN$^+$02]. An elastic force model was also derived for the elastic potential energy of a system in which, for simplicity, virtual linear springs were arranged in a radial pattern inside hemispherical soft fingertips. Doulgeri *et al.* discussed the problem of stable grasping with deformable fingertips on which rolling constraints were described as nonholo-

nomic because of the change in the effective rolling radius of the soft fingertip [DFA02, DF03]. The above-mentioned studies, however, focused mainly on deriving a control law to realize stable grasping and attitude control of the grasped object rather than on revealing a physically appropriate deformation model, which also contains the nonlinear characteristics of a hemispherical soft fingertip.

On the other hand, Xydas *et al.* proposed an exact deformation model based on the mechanics of materials having nonlinear characteristics and performed finite element analysis (FEA) for a hemispherical soft fingertip [XK99, XBK00]. Kao *et al.* experimentally demonstrated that the elastic force due to deformation satisfied a power law with respect to the displacement of the fingertip and insisted that their theory subsumed Hertzian contact [KY04]. These studies, however, did not distinguish between the material nonlinearity of the soft fingertip and the geometric nonlinearity caused by the hemispherical shape of the fingertip; they also defined a parameter that accounts for the effects of both nonlinearities. Consequently, the cause of the discrepancy between the results of the simulation based on their model and the results of actual experiments was not apparent. In addition, as a result of the complexity of these models, these studies do not generally lend themselves to the analysis of equations of motion for a soft-fingered manipulation system. While FEA may enable us to derive a stress distribution and an elastic force on the soft fingertip, these simulation results depend on the selected mesh pattern. Although FEA based on a certain arbitrary mesh pattern may prove the stability for equations of motion of the handling system, it does not always provide proof of stability for equations derived from other mesh patterns.

We herein propose a static elastic model of a hemispherical soft fingertip in a physically reasonable and straightforward form suitable for theoretical analysis of robotic handling motions. This model is assumed to be composed of 1D linear springs placed within a hemispherical soft fingertip that stand perpendicularly on the bottom and is called a *parallel-distributed model*. We distinguish between geometric nonlinearity due to the hemispherical shape and material nonlinearity of soft materials, *i.e.,* the nonlinearity of the Young's modulus of the soft material, allowing us to focus only on the geometric nonlinearity of the soft fingertip and analytically formulate the elastic force and elastic potential energy equations for the deformation of the fingertip. We show that each equation is a function of two variables: the maximum displacement of the fingertip and the orientation angle of the contacted object. We also show that when the object is positioned normal to the fingertips, the elastic potential energy is minimal. Finally, we validate the static elastic model by conducting a compression test of the hemispherical soft fingertip and evaluating the results.

3.2 Static Elastic Model of a Hemispherical Soft Fingertip

3.2.1 Fingertip Stiffness

We treat the fingertips as if they were composed of an infinite number of virtual linear springs that are standing vertically. Figure 3.1 shows one such spring. We formulate elastic force and elastic potential energy equations for the deformation of the fingertip. In order to simplify the derivation process of both equations, two assumptions associated with material characteristics are given as follows: (1) The incompressibility of elastomer materials is not considered and (2) Young's modulus is assumed to be constant. Note that the contact condition being discussed in the present study is restricted to the case in which a force applied to the fingertip is assumed to be along the z-axis of the fingertip. In addition, we assume that the object never comes into contact with the bottom plane of the fingertip.

Let us apply an infinitesimal virtual spring QR with sectional area $\mathrm{d}S$ inside the soft fingertip, as shown in Fig. 3.1. Let $\mathrm{d}F$ be the infinitesimal elastic force due to the shrinkage PQ of the virtual spring. Let θ_p be the orientation angle of the contacting object, and let a be the fingertip radius. Let d be the maximum displacement of the fingertip, and let $a_\mathrm{c} = \sqrt{a^2 - (a-d)^2}$ be the radius of the contacting circle. Let P be the point at which the spring is in contact with the object. Finally, let θ be the angle subtended between line PQ and the z-axis, and let ϕ be the azimuthal angle on the xy-plane. Using the contact surface equation, $x \sin\theta_\mathrm{p} + z\cos\theta_\mathrm{p} = a - d$ (Appendix A.1), the length of PR is then expressed as

$$\mathrm{PR} = \frac{a - d - x\sin\theta_p}{\cos\theta_p}. \tag{3.1}$$

Since the length of QR becomes $\sqrt{a^2 - (x^2+y^2)}$ due to the hemispherical feature, the infinitesimal elastic force $\mathrm{d}F$ on a single virtual spring QR is given by

$$\mathrm{d}F = k \cdot \mathrm{PQ} = k\left\{\sqrt{a^2-(x^2+y^2)} - \frac{a-d-x\sin\theta_\mathrm{p}}{\cos\theta_\mathrm{p}}\right\}, \tag{3.2}$$

where k is the linear spring constant of the spring QR. Note that k is proportional to the sectional area $\mathrm{d}S$ and inversely proportional to the natural length $\sqrt{a^2-(x^2+y^2)}$. Letting E be Young's modulus of soft-finger materials, k is described as (Appendix A.2)

$$k = \frac{E\,\mathrm{d}S}{\sqrt{a^2-(x^2+y^2)}}. \tag{3.3}$$

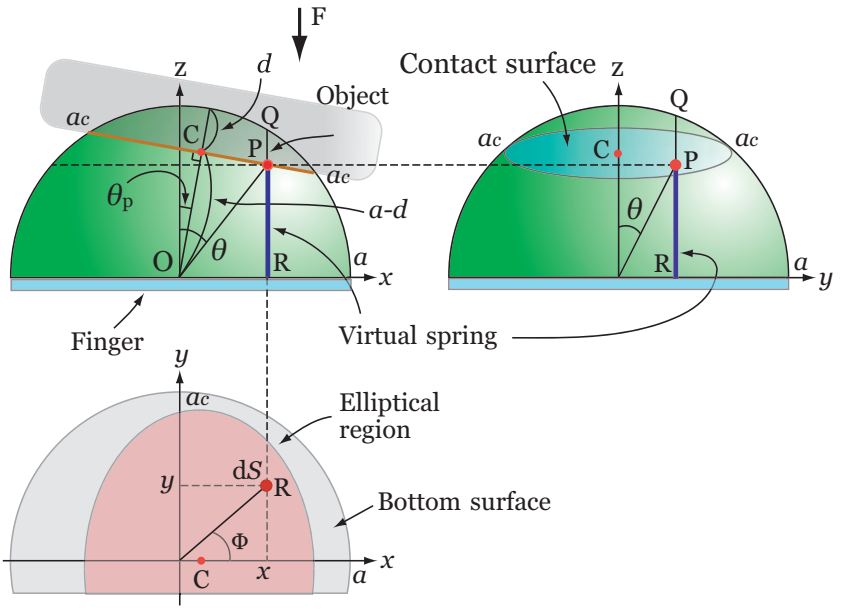

Fig. 3.1 Contact mechanism

Letting K be the fingertip stiffness on the entire deformed part illustrated in Fig. 3.1, based on Eq. 3.3, K can be expressed as

$$K = \int_{ell} k = E \int_{-a_c}^{a_c} \int_{b_1(y)}^{b_2(y)} \frac{\mathrm{d}x\,\mathrm{d}y}{\sqrt{a^2 - (x^2 + y^2)}}, \tag{3.4}$$

where

$$b_1(y) = (a-d)\sin\theta_\mathrm{p} - \cos\theta_\mathrm{p}\sqrt{a_\mathrm{c}^2 - y^2}, \tag{3.5}$$

$$b_2(y) = (a-d)\sin\theta_\mathrm{p} + \cos\theta_\mathrm{p}\sqrt{a_\mathrm{c}^2 - y^2}, \tag{3.6}$$

and *ell* denotes the elliptical region shown in Fig. 3.2. Applying a numerical integration to Eq. 3.4, we find that the fingertip stiffness is almost constant with respect to the object orientation, which is depicted as continuous lines, as shown in Fig. 3.3. This occurs even when the maximum displacement d changes several values. This indicates that the fingertip stiffness K is independent of the object orientation θ_p. Hence, in the present study we need a third assumption: (3) The fingertip stiffness is independent of the object orientation as long as the maximum displacement remains constant. Using the above numerical assumption, we formulate the fingertip stiffness K as an analytical formula.

Next, performing the substitution whereby $x = r\cos\phi\cos\theta_\mathrm{p} + (a-d)\sin\theta_\mathrm{p}$ and $y = r\sin\phi$, Eq. 3.4 is then transformed into (Appendix A.3)

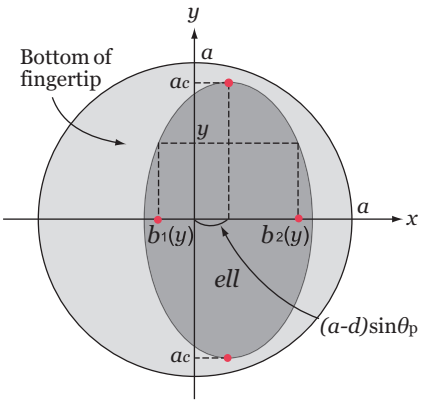

Fig. 3.2 Integration area obtained by projecting the contact plane onto the xy-coordinate

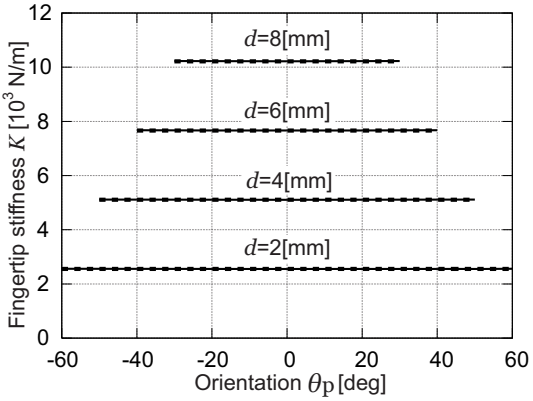

Fig. 3.3 Comparison between the numerical results of Eq. 3.4 (*continuous lines*) and analytical simulations of Eq. 3.8 (*dotted lines*) for $E = 0.2032$ MPa

$$K = E \int_0^{a_c} r \left\{ \int_0^{2\pi} \frac{\cos\theta_p \, \mathrm{d}\phi}{\sqrt{a^2 - \{x^2(r,\phi) + y^2(r,\phi)\}}} \right\} \mathrm{d}r$$
$$= E \int_0^{a_c} r \int_0^{2\pi} B(r,\phi) \mathrm{d}\phi \, \mathrm{d}r. \tag{3.7}$$

Since assumption (3) requires that K is independent of θ_p, we can substitute $\theta_p = 0$ into Eq. 3.7 and obtain

$$K = E \int_0^{a_c} r \left\{ \int_0^{2\pi} \frac{\mathrm{d}\phi}{\sqrt{a^2 - r^2}} \right\} \mathrm{d}r = 2\pi E d. \tag{3.8}$$

Plotting the simulation result of Eq. 3.8 as dotted lines onto Fig. 3.3 together with the results of Eq. 3.4, we find that these lines coincide with each other. This implies that the third assumption due to the numerical observation is appropriate, and the stiffness is a function of only the maximum displacement d.

3.2.2 Elastic Force

Likewise, using the third assumption associated with the fingertip stiffness, we formulate the elastic force and potential energy equations in a straightforward manner. Using Eqs. 3.2 and 3.3, and a geometric relationship $\mathrm{QT} = \mathrm{PQ}\cos\theta_\mathrm{p}$ (Fig. A.2 in Appendix A.3), the elastic force F on the total deformed region can be written as

$$\begin{aligned} F &= \int_{ell} k\mathrm{PQ} = \frac{1}{\cos\theta_\mathrm{p}} \int_{ell} k \cdot \mathrm{QT} \\ &= \frac{E}{\cos\theta_\mathrm{p}} \int_{-a_\mathrm{c}}^{a_\mathrm{c}} \int_{b_1(y)}^{b_2(y)} \frac{\mathrm{QT}(x,y)\,\mathrm{d}x\,\mathrm{d}y}{\sqrt{a^2-(x^2+y^2)}}. \end{aligned} \tag{3.9}$$

Performing the same variable conversion between the (x, y)-coordinate and the (r, ϕ)-coordinate used in the derivation process of K, Eq. 3.9 is then transformed as

$$F = \frac{E}{\cos\theta_\mathrm{p}} \int_0^{a_\mathrm{c}} \mathrm{QT}(r) \cdot r \left\{ \int_0^{2\pi} B(r,\phi)\,\mathrm{d}\phi \right\} \mathrm{d}r, \tag{3.10}$$

where (Fig. A.2)

$$\mathrm{QT}(r) = \sqrt{a^2 - r^2} - (a - d). \tag{3.11}$$

In Eq. 3.10, $B(r, \phi)$ corresponds to the integrand within the braces in Eq. 3.7. Here, applying assumption (3) to $B(r, \phi)$ as well as Eq. 3.8, F is finally calculated as

$$F = \frac{E}{\cos\theta_\mathrm{p}} \int_0^{a_\mathrm{c}} \mathrm{QT}(r) \cdot r \left\{ \int_0^{2\pi} \frac{\mathrm{d}\phi}{\sqrt{a^2-r^2}} \right\} \mathrm{d}r = \frac{\pi E d^2}{\cos\theta_\mathrm{p}}. \tag{3.12}$$

Thus, we can obtain a straightforward equation that will be applicable to the analytical validation for manipulation due to the simplicity.

3.2.3 Elastic Potential Energy

Note that Eqs. 3.12 and 3.15 indicate that the elastic force and elastic potential energy on the entire deformed part of a hemispherical soft fingertip are functions of two variables, namely, the maximum displacement d and the object orientation angle θ_p. Furthermore, we find that both formulae have a local minimum when the orientation angle remains zero. In particular, we describe the minimum value of elastic energy as the *local minimum of elastic potential energy* (*LMEE*).

In addition to Eq. 3.9, the elastic potential energy P on the entire deformed region is expressed as

$$\begin{aligned} P &= \frac{1}{2}\int_{ell} k\mathrm{PQ}^2 = \frac{1}{2\cos^2\theta_\mathrm{p}}\int_{ell} k\cdot\{\mathrm{QT}(x,y)\}^2 \\ &= \frac{E}{2\cos^2\theta_\mathrm{p}}\int_{-a_\mathrm{c}}^{a_\mathrm{c}}\int_{b_1(y)}^{b_2(y)} \frac{\{\mathrm{QT}(x,y)\}^2\mathrm{d}x\,\mathrm{d}y}{\sqrt{a^2-(x^2+y^2)}}. \end{aligned} \tag{3.13}$$

Performing the same variable conversion between the (x,y)-coordinate and the (r,ϕ)-coordinate used in the derivation process of F, Eq. 3.13 is then transformed as

$$P = \frac{E}{2\cos^2\theta_\mathrm{p}}\int_0^{a_\mathrm{c}} \{\mathrm{QT}(r)\}^2\cdot r\left\{\int_0^{2\pi} B(r,\phi)\,\mathrm{d}\phi\right\}\mathrm{d}r. \tag{3.14}$$

Again, applying assumption (3) to $B(r,\phi)$ in Eq. 3.14, P is finally calculated as

$$\begin{aligned} P &= \frac{E}{2\cos^2\theta_\mathrm{p}}\int_0^{a_\mathrm{c}} \mathrm{QT}^2(r)\cdot r\left\{\int_0^{2\pi}\frac{\mathrm{d}\phi}{\sqrt{a^2-r^2}}\right\}\mathrm{d}r \\ &= \frac{\pi E d^3}{3\cos^2\theta_\mathrm{p}}. \end{aligned} \tag{3.15}$$

Finally, in order to confirm the transformations of formulae from Eq. 3.9 to Eq. 3.12 and from Eq. 3.13 to Eq. 3.15, we compare the numerical analysis of Eqs. 3.9 and 3.13 with the simulation results of Eqs. 3.12 and 3.15. Figure 3.4 shows a good result, and concludes that both Eqs. 3.12 and 3.15 are mathematically reasonable formulae in the present study.

3.2.4 Relationship Between Elastic Force and Elastic Energy

While the individual virtual spring used in the present study is based on a linear elasticity, the entire fingertip model obtained by completing the double

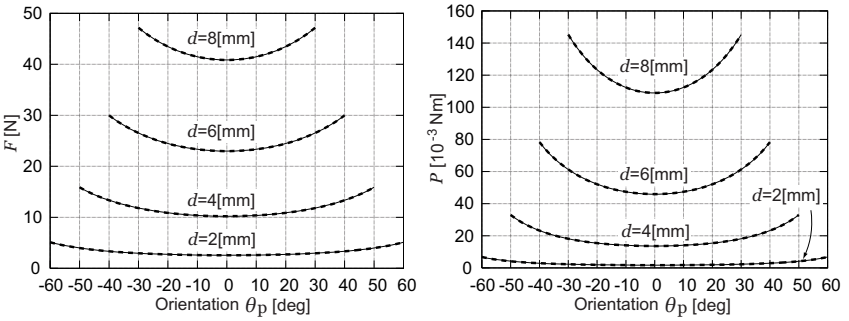

(**a**) Elastic force (**b**) Elastic energy

Fig. 3.4 Comparison between the numerical integration and the analytical simulation of F and P, respectively. The *continuous lines* correspond to the numerical results of Eqs. 3.9 and 3.13, and the *dotted lines* correspond to the analytical results of Eqs. 3.12 and 3.15

integration on an elliptical region exhibits a geometric nonlinearity caused by the hemispherical shape of the fingertip. In other words, the completed fingertip model has a variable fingertip stiffness with respect to d, which is expressed as Eq. 3.8. Hence, when we compute the total force Eq. 3.12 from the energy Eq. 3.15, we must define an *equivalent displacement* to be used for the differential calculation.

In the case of normal contact corresponding to $\theta_\mathrm{p} = 0$ in Eq. 3.15, elastic models are given as follows:

$$P = \frac{\pi E d^3}{3}, \tag{3.16}$$

$$\frac{\partial P}{\partial d} = \pi E d^2 = F, \tag{3.17}$$

$$\frac{\partial^2 P}{\partial d^2} = 2\pi E d = K, \tag{3.18}$$

where d corresponds to the equivalent displacement. Next, let us consider the case of diagonal contact when $\theta_\mathrm{p} \neq 0$. We define Δz_{eq} as an equivalent displacement, which must satisfy

$$\frac{\partial P}{\partial \Delta z_{eq}} = \frac{1}{3}\frac{\partial \left(\pi E \Delta z_{eq}^3 \cos\theta_\mathrm{p}\right)}{\partial \Delta z_{eq}} = \pi E \Delta z_{eq}^2 \cos\theta_\mathrm{p} = \frac{\pi E d^2}{\cos\theta_\mathrm{p}} = F, \tag{3.19}$$

$$\frac{\partial^2 P}{\partial \Delta z_{eq}^2} = \frac{\partial \left(\pi E \Delta z_{eq}^2 \cos\theta_\mathrm{p}\right)}{\partial \Delta z_{eq}} = 2\pi E \Delta z_{eq} \cos\theta_\mathrm{p} = 2\pi E d = K. \tag{3.20}$$

The displacement Δz_{eq} to fulfill Eqs. 3.19 and 3.20 can be found such that a geometric relationship $d = \Delta z_{eq} \cos\theta_\mathrm{p}$ is maintained as shown in Fig. A.2.

Δz_{eq} is the true maximum displacement among all of the virtual springs in any case that includes $\theta_{\mathrm{p}} = 0$ and $\theta_{\mathrm{p}} \neq 0$.

3.3 Comparison with Hertzian Contact

In 1881, Hertz proposed a contact theory for two elastic objects having arbitrary curved surfaces [Joh85]. He showed that a normal contact force generated between an elastic sphere and a plane, whose Young modulus is infinity, can be expressed as

$$F = \frac{4\sqrt{R}}{3}\left(\frac{E}{1-\nu^2}\right) d^{\frac{3}{2}}, \tag{3.21}$$

where R is the radius, E is the Young modulus of the object, ν is the Poisson ratio, and d is the maximum displacement of the sphere. Since the above equation is useful from a practical viewpoint, it has been widely used for computing the contact stress between, for example, a wheel and a rail, a roll and material, or a retainer and a ball in a bearing. However, in Hertzian contact, it is assumed that both elastic objects are open elliptic paraboloids with an arbitrary radius of curvature. Consequently, no boundary conditions are used in the Hertzian contact model.

Kao *et al.* defined the parameter c_d corresponding to a material and geometric nonlinearity [KY04] and transformed Eq. 3.21 into

$$F = c_d d^{\zeta}. \tag{3.22}$$

They conducted a vertical compression test using a hemispherical soft fingertip and estimated the parameter c_d empirically using a weighted least-squares method (LSM). It has been shown that ζ is approx. 2.3 or 1.75 when the rate of deformation of the finger is above or below 20%, respectively. In other words, the parameter ζ is not identical to 3/2 in the contact model of soft fingertips. Thus, the Hertzian contact theory cannot be adopted for deriving the elastic model of the hemispherical soft fingertip.

Figure 3.5 shows a comparison result in which the elastic force value with respect to the displacement d is plotted when a hemispherical soft fingertip of radius 20 mm is compressed vertically. The vertically oriented spring model is more suitable for deriving an elastic force up to the midrange displacement of the fingertip. This is because our model contains a geometric nonlinearity due to the hemispherical shape of the fingertip, that is, the present model indicates that ζ becomes not 3/2, but 2, which appears within 1.75 and 2.3, only by adopting an appropriate natural length for the individual springs.

Soft materials exhibit nonlinear characteristics, even for infinitesimal deformations. Tatara newly derived a nonlinear Young's modulus with respect to compressive strain [Tat91]. Furthermore, the concept of the contact angle

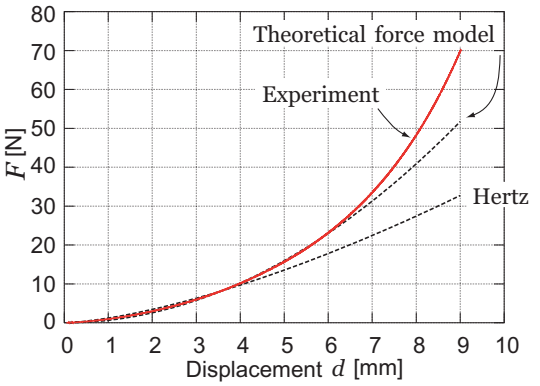

Fig. 3.5 Comparison between the Hertzian contact model and the present elastic force model (Eq. 3.12) when $\theta_{\mathrm{p}} = 0$ and $E = 0.2032$ MPa obtained by a corresponding identification test mentioned in the next section

of the object is not incorporated in the Hertzian contact theory. While the Hertzian contact theory can be used for a simple contact pattern corresponding to the normal contact, no contact at any other arbitrary angle or rolling contact can be defined. On the other hand, the elastic models proposed in this chapter cover any contact angle of the object, and therefore, these models can be used to analyze grasping and manipulating motions for various possible types of contact by a soft-fingered robotic hand.

3.4 Measurement of Young's Modulus

In the present study, the Young modulus of the soft fingertip was measured by conducting a compression test on six cylinders of polyurethane gel. Three cylinders were 20 mm in diameter and 15, 20, and 25 mm in height, and three were 30 mm in diameter and 15, 20, and 25 mm in height, as shown in Fig. 3.6a.

Figure 3.7a shows an overall view of a measured stress-strain diagram, and an enlarged view of part of the diagram is shown in Fig. 3.7b. The numerical values shown in both graphs denote the specimen height on the left side and the specimen diameter on the right side. The data were averaged and smoothed using the LSM, as shown in Fig. 3.8. We assumed the maximum deformation of the soft fingertip to be 50% of the radius. Furthermore, in order to focus predominantly on the geometric nonlinearity due to the hemispherical shape, we did not consider the material's nonlinearity, which, for soft materials, is directly related to the Young's modulus. Consequently, we performed a linear approximation for a 50% strain, as in Fig. 3.8 and estimated the Young modulus as 0.2032 MPa.

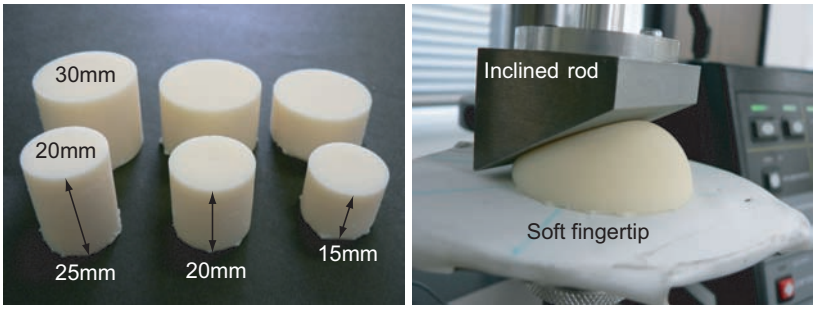

(**a**) Several specimens (**b**) Compression test

Fig. 3.6 Compression test of a hemispherical soft fingertip

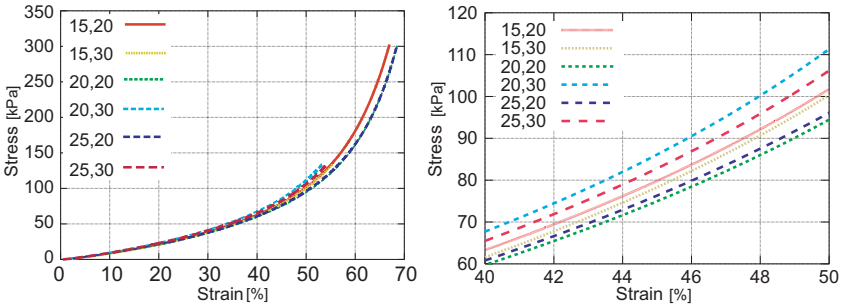

(**a**) Stress-strain diagram (**b**) Enlarged view

Fig. 3.7 Stress-strain diagram of polyurethane rubber

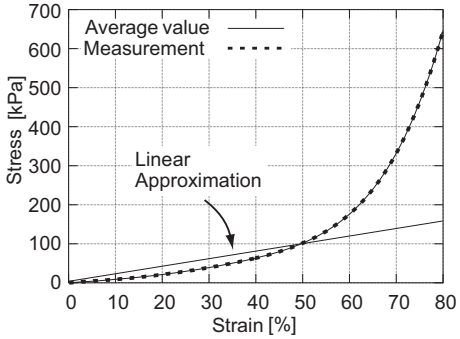

Fig. 3.8 Average value of stress-strain diagram

3.5 Compression Test

By compressing a hemispherical soft fingertip made of polyurethane gel along the normal direction, as shown in Figs. 3.1 and 3.6b, we verified the validity of the elastic force model represented in Eq. 3.12. Furthermore, by conducting

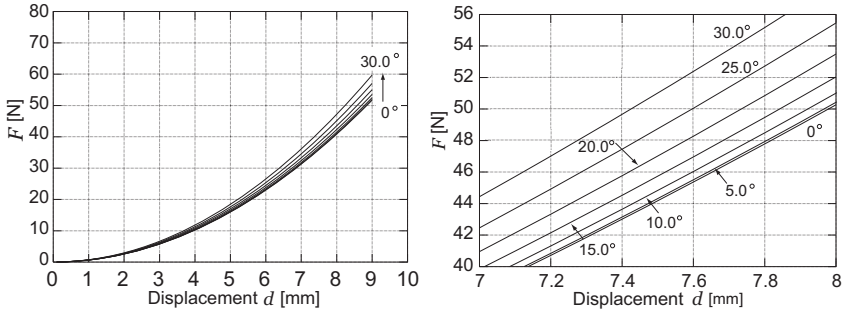

(**a**) Simulations (**b**) Enlarged view

Fig. 3.9 Simulation results of elastic force

multiple experiments with various contacting angles, we demonstrated the existence of the local minimum of the elastic force. In the compression test, we used a fingertip with a diameter of 40 mm and contacting rods of 13 different shapes. The rods were inclined from 0 to 30° in increments of 2.5°, as shown in Fig. 3.6b. Figure 3.10 compares the experimental results with the simulation results. The horizontal axis represents the maximum displacement of the compressed fingertip, while the vertical axis represents the elastic force measured by a load cell placed in the compression machine.

In all of the graphs in Fig. 3.10, the simulation and experimental results are almost identical up to $d = 6.0$ mm, after which the discrepancies increase with the magnitude of the displacement. The discrepancies stem from the linear approximation of the experimental stress-strain diagram shown in Fig. 3.8. The effect leads directly to the nonlinearity of Young's modulus, which is outside the scope of the present study.

Figure 3.9a and 3.11a show the simulation and experimental results, respectively. Enlarged views of both results are also shown in Figs. 3.9b and 3.11b. The numerical values in each graph denote the inclined angle of the contacted object, and both results are plotted at intervals of 5.0°. The elastic force increases as the orientation angle increases under constant maximum displacement. For confirmation, we plotted the elastic force with respect to θ_{p} of Eq. 3.12 in Fig. 3.12 together with the Hertzian contact model and the radially-distributed model derived by Arimoto's group. The numerical values shown in the graph denote the maximum displacement d. Note that the Hertzian force is depicted at a point because the model does not define the object orientation. At approx. 0°, there is a clear local minimum of the elastic force, and the change in elastic force with respect to θ_{p} is greatest when the displacement is maximum, that is, 8.0 mm. The same tendency can also be seen in the simulation results. The results therefore indicate that the proposed elastic model is able to represent a distinctive phenomenon, *i.e.,* a local minimum elastic force, even when the derivation process is represented simply using linear virtual springs aligned in the normal direction. On the

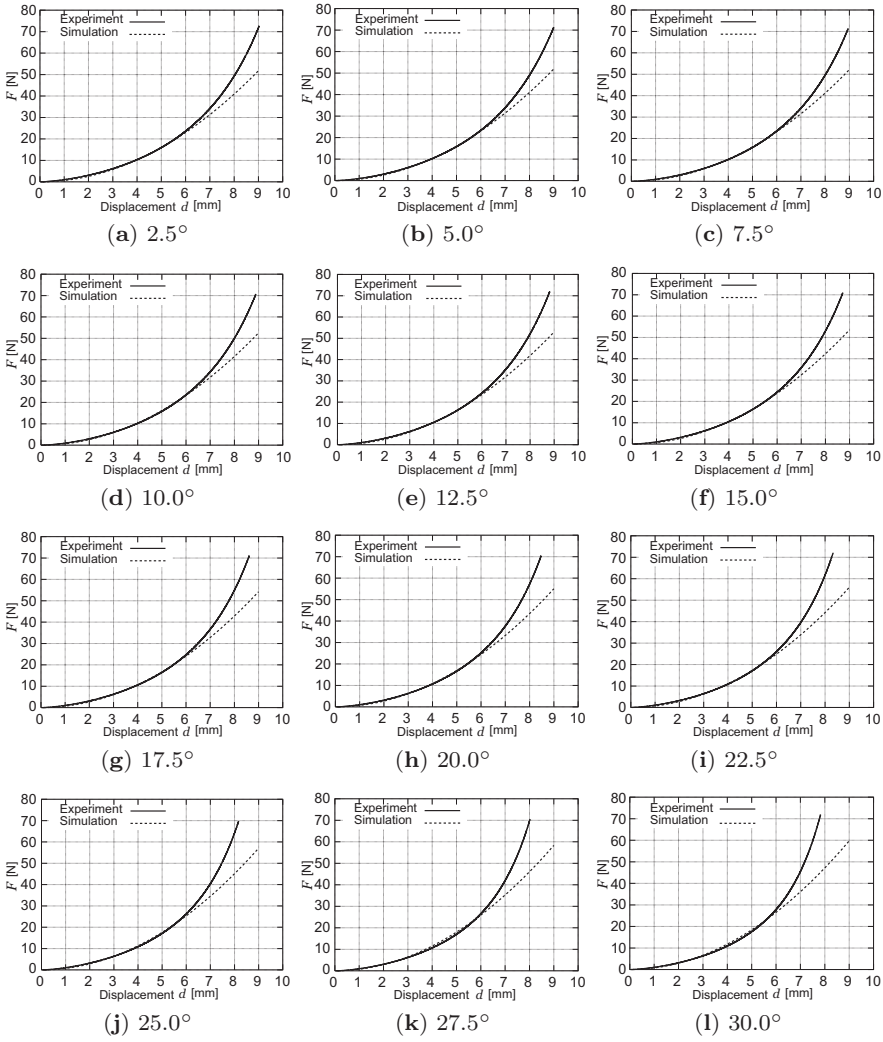

Fig. 3.10 Elastic forces in experiments

other hand, the discrepancy in the large displacement shown in Fig. 3.12 would be reduced if the Young modulus could be defined as a nonlinear function of compression strain and be used to adopt the model to accommodate the nonlinearity of the material. However, this elastic force model focuses on the geometric nonlinearity, and the derivation process including both nonlinearities will be addressed in Chap. 9.

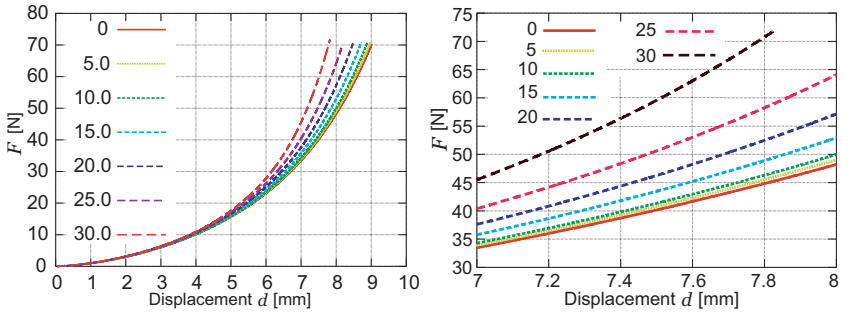

(**a**) Experiments (**b**) Enlarged view

Fig. 3.11 Experimental results of elastic force

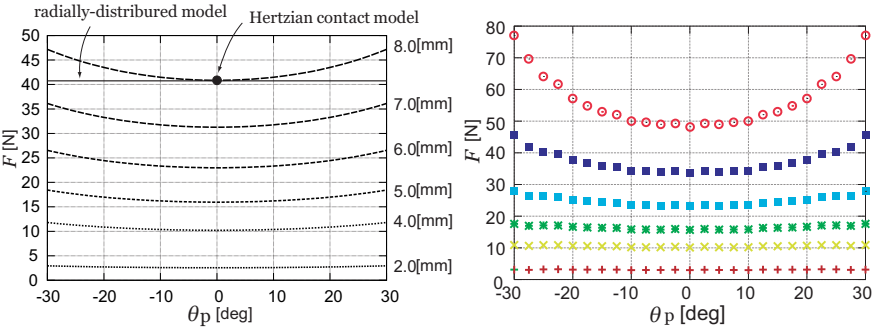

(**a**) Simulations (**b**) Experiments

Fig. 3.12 Local minimum of elastic force

3.6 Concluding Remarks

We have proposed a parallel-distributed fingertip model, a static 1D elastic force model, and formulated an elastic potential energy function based on virtual springs inside a hemispherical soft fingertip. We have also proven the existence of an LMEE and experimentally demonstrated that the elastic force due to the deformation has a local minimum. The proposed model requires only the measurement of the Young's modulus of a corresponding material to be used in robotic fingertips. In future studies, we will consider the constant-volume deformation of incompressible elastomer materials and derive elastic models incorporating a nonlinear elasticity.

By expanding the new concept of LMEE in the development of grasping and manipulation theory using a soft-fingered robotic hand, it is expected that the stable grasping and the pose control of a grasped object by a minimal-DOF two-fingered hand may be achieved and a succinct control system will be designed.

http://www.springer.com/978-1-84800-980-6

Mechanics and Control of Soft-fingered Manipulation
Inoue, T.; Hirai, S.
2009, XVIII, 245 p., Hardcover
ISBN: 978-1-84800-980-6